Neutron Flux Distribution on the Wall of Toroidal
Controlled Thermonuclear Reactor Devices with
Elongated Cross Section

G. Becker and R. Wunderlich

IPP 1/143 Februar 1974

MAX-PLANCK-INSTITUT FÜR PLASMAPHYSIK

GARCHING BEI MÜNCHEN

MAX-PLANCK-INSTITUT FÜR PLASMAPHYSIK

GARCHING BEI MÜNCHEN

Neutron Flux Distribution on the Wall of Toroidal
Controlled Thermonuclear Reactor Devices with
Elongated Cross Section

G. Becker and R. Wunderlich

IPP 1/143　　　　G. Becker　　　　Neutron Flux Distribution on the Wall

　　　　　　　　　R. Wunderlich　　　of Toroidal Controlled Thermonuclear

　　　　　　　　　　　　　　　　　Reactor Devices with Elongated Cross

　　　　　　　　　　　　　　　　　Section.

　　　　　　　　　　　　　　　　　(in English)

　　　　　　　　　　　　　　　　　February 1974

Abstract:

　　The neutron flux distribution on the wall of a toroidal CTR device with strongly elongated cross section is calculated. On the inner and outer cylindrical walls (belt-pinch device) the flux distribution has a plateau region with a half-width equal to about the height of the plasma. The maximum flux is found on the outer cylinder and in the symmetry plane ($z_o = 0$). The neutron flux asymmetry and reduction η of the mean wall loading are determined. For standard data an η of 57 % is computed. This is mainly due to the flux profiles on the cylindrical walls and does not depend sensitively on the toroidal curvature. For standard parameters the inner cylinder absorbs 22.6 %, the outer cylinder 68.6 % and the end plates together 8.8 % of the total neutron emission. The corresponding values for a straight device with the same coil and plasma cross section are 44 %, 44 % and 12 %. A reduction of toroidal curvature diminishes flux asymmetry between the inner and outer cylinders. The maximum flux and minimum η-value are obtained at a large torus radius equal to two times the coil width.

1. INTRODUCTION

In designing the blanket of a special thermonuclear reactor device like that with an axisymmetric configuration and elongated cross section, one important question is whether there are large asymmetries in the flux of fast neutrons. Another aspect is the possibility of large localized wall loading by energetic neutrons due to asymmetries. It is obvious that the neutron flux distribution on the wall will depend both on the geometry of the neutron source (plasma) and on the wall geometry. Simple solid angle arguments yield only very rough estimates. Therefore, a detailed numerical calculation is made in order to obtain quantitative results.

2. METHOD OF CALCULATION

For the sake of simplicity it is assumed that the intensity ε of the source of energetic neutrons is homogeneous, and that the plasma has a rectangular cross section (see Fig.1). Experimental plasmas have a racetrack-like shape. Both idealizations should be very good approximations of reality. Here ε is defined as the number of neutrons per sec that are emitted by 1 cm^3 of the source. It is further assumed that the wall and blanket systems is an ideal neutron absorber in the sense that no neutrons are reflected after hitting the wall. The neutron flux Φ is defined as the number of neutrons per cm^2 and per sec. With a constant ε throughout the plasma and a plasma volume V_p (see Fig.1, $R_t = \frac{1}{2}(R_i + R_e)$)the total neutron emission is

$$\Psi_{tot} = V_p \cdot \varepsilon = 4\ ab\ 2\pi\ R_t \cdot \varepsilon \tag{1}$$

The neutron flux distribution on the wall is calculated by using Fig. 2. A point P_o on the wall is defined by the coordinates x_o, y_o, z_o, whereas a point P within the plasma has the coordinates x, y, z. The distance ℓ between P_o and P is then given by

$$\ell^2 = (x - x_o)^2 + (y - y_o)^2 + (z - z_o)^2 \tag{2}$$

The appropriate coordinates are, of course, cylindrical coordinates r, φ and z

$$x = r\cos\varphi \qquad y = r\sin\varphi \qquad z = z$$

Because of the axisymmetry of the problem one need only calculate the flux distribution on the wall in a meridional plane $\varphi = 0$, i.e. for $y_o = 0$. One thus obtains from Eq. (2)

$$\ell^2 = (r \cos \varphi - r_o)^2 + r^2 \sin^2 \varphi + (z - z_o)^2 \tag{3}$$

For $x_o = r_o$ one must insert R_i for the inner cylinder and R_e for the outer cylinder. The angle α between the normal vector of a surface element df_o on the wall and the vector $\vec{\ell}$ is given by

$$\cos \alpha = \frac{r \cos \varphi - r_o}{\ell}$$

Therefore, the projection of df_o onto a plane perpendicular to $\vec{\ell}$ reads

$$df = df_o \frac{r \cos \varphi - r_o}{\ell}$$

It can be used to determine the element $d\Omega$ of the solid angle in which df_o appears as seen from a point P in the plasma:

$$d\Omega = \frac{df}{\ell^2} = df_o \frac{r \cos \varphi - r_o}{\ell^3} \tag{4}$$

The neutrons are emitted isotropically by a plasma element. This means that the number of neutrons which pass through df_o per sec, and which come from a volume element dV of the source is given by $d\Phi(r_o; z_o) df_o = \frac{d\Omega}{4\pi} dV \cdot \varepsilon$

With $dV = r \, dr \, d\varphi \, dz$ one obtains for the inner and outer cylinders, by substituting Eqs. (3) and (4)

$$d\Phi(r_o; z_o) = \frac{\varepsilon}{4\pi} \frac{(r \cos \varphi - r_o) \, r \, dr \, d\varphi \, dz}{\left[(r \cos \varphi - r_o)^2 + r^2 \sin^2 \varphi + (z - z_o)^2 \right]^{3/2}} \tag{5}$$

The integration between $z = -b$ and $z = b$ yields

$$\phi(r_o; z_o) = \frac{\varepsilon}{4\pi} \int_{R=R_t-a}^{R_t+a} \int_{\varphi = -\varphi_m}^{\varphi_m} \frac{1}{k^2} \left[\frac{b - z_o}{\sqrt{(b-z_o)^2 + k^2}} + \frac{b + z_o}{\sqrt{(b+z_o)^2 + k^2}} \right] (r \cos \varphi - r_o) \, r \, dr \, d\varphi \tag{6}$$

with $k^2 = (r \cos \varphi - r_o)^2 + r^2 \sin^2 \varphi$.

Here φ_m is the limiting angle of the φ-integration. It can be derived from Fig. 2 for the inner and outer cylinders.

a) Inner cylinder $r_o = R_i$:

$$\varphi_m(r) = \cos^{-1}\left(\frac{R_i}{r}\right) \tag{7}$$

b) Outer cylinder $r_o = R_e$:

$$\varphi_m(r) = \varphi_1 + \varphi_2 \quad \text{with} \quad \varphi_1 = \cos^{-1}\left(\frac{R_i}{R_e}\right) \quad \text{and} \quad \varphi_2 = \cos^{-1}\left(\frac{R_i}{r}\right)$$

and therefore

$$\varphi_m(r) = \cos^{-1}\left[\frac{1}{rR_e}\left(R_i^2 - \sqrt{R_e^2 - R_i^2}\sqrt{r^2 - R_i^2}\right)\right] \tag{8}$$

The result for the top or bottom plate that corresponds to Eq. (6) reads

$$\Phi\left(r_o; z_o = \pm\frac{H}{2}\right) = \frac{\epsilon}{4\pi} \int_{z=\frac{H}{2}-b}^{\frac{H}{2}+b} \int_{r=R_t-a}^{R_t+a} \int_{\varphi=-\varphi_m}^{\varphi_m} \frac{z\, r\, dr\, d\varphi\, dz}{(k^2 + z^2)^{3/2}} \tag{9}$$

with a limiting angle

$$\varphi_m(r) = \cos^{-1}\left[\frac{1}{r\, r_o}\left(R_i^2 - \sqrt{r_o^2 - R_i^2}\sqrt{r^2 - R_i^2}\right)\right] \tag{10}$$

3. RESULTS

The integration of Eqs.(6) and (9) is performed numerically for $\epsilon = 1$. For the standard parameters of a belt-pinch reactor proposal (see Fig.1) one obtains the flux distribution shown in Fig.3. The standard data normalized to the coil width $W = R_e - R_i$ are :

Coil geometry: $\dfrac{R_i}{W} = 1, \quad \dfrac{R_e}{W} \simeq 2, \quad \dfrac{H}{W} = 6$

Plasma geometry: $\dfrac{a}{W} = 0.2, \quad \dfrac{b}{W} = 2.0, \quad \dfrac{R_t}{W} = \dfrac{R_i + R_e}{2W} = 1.5$

Obviously, the flux distributions on the inner and on the outer cylinder are qualitatively very similar. Both have a plateau region which is symmetric to the $z_o = 0$ plane with a half-width of about $2\,b$. The flux on the outer cylinder, however, exceeds the corresponding values on the inner cylinder for all z_o. The ϕ- values are relatively small on the top and bottom plates. The largest flux occurs at $r_o = R_e$ and $z_o = 0$ ($\phi\,(R_e;\,0)$).

The difference between the local flux $\phi\,(r_o;\,z_o)$ and the averaged flux ϕ_{av} is a measure of the asymmetry Δ of the flux distribution. The asymmetry is defined as

$$\Delta\,(r_o;\,z_o) = \frac{\phi(r_o;\,z_o) - \phi_{av}}{\phi_{av}} = \frac{\phi\,(r_o;\,z_o)}{\phi_{av}} - 1 \tag{11}$$

where ϕ_{av} is given by the ratio of total neutron emission ψ_{tot} of the plasma (see Eq. (1)) and total coil surface $F = 2\,\pi\,R_t\,2\,(H + R_e - R_i)$ for $R_t = \dfrac{1}{2}\,(R_i + R_e)$

$$\phi_{av} = \frac{\psi_{tot}}{F} = \frac{2\,ab\,\epsilon}{H + R_e - R_i} \tag{12}$$

The asymmetry factor Δ for the standard case is shown in Fig.4. It is obvious from this figure that the flux is smaller than ϕ_{av} in a region of the wall with $|z_o| > b$ including the end plates. On the outer cylinder there are large regions with a flux clearly above ϕ_{av}, i.e. these regions have to withstand the strong wall loading.

Another important quantity is the reduction factor η of the mean wall loading due to flux asymmetry. In the case of an everywhere constant flux the wall can withstand $\phi_m \cdot F$ neutrons per sec, where ϕ_m is the maximum flux possible on the wall. With an asymmetric distribution, however, ϕ_m can be reached only locally because the maximum $\phi\,(r_o = R_e;\,z_o = 0)$ must not exceed ϕ_m.

One therefore defines

$$\eta = \frac{\Psi_{tot}}{\phi_m \cdot F} = \frac{\phi_{av}}{\phi(R_e \, ; \, 0)} \qquad (13)$$

For the standard case η is found to be 0.57.

The dependence of the flux distribution on the plasma geometry has been discussed above. We are now interested in the question how the toroidal equilibrium position effects the flux asymmetry. It is intuitively clear that devices with strongly elongated cross sections are favourable in so far as their flux asymmetry (z_o - de - pendence) on the inner cylinder or on the outer cylinder does not depend sensitively on the toroidal equilibrium position of the plasma. The main effect is a change of flux asymmetry between the inner and outer cylinders.

In order to learn how the flux asymmetry depends on the toroidal curvature of the device, the torus radius R_t ($R_t = \frac{1}{2}(R_i + R_e)$) is varied with the coil and plasma cross section kept fixed($W=R_e-R_i$, H, a and b as in the standard case). In Fig. 5 the fluxes in the plane $z_o = 0$ on the inner and outer cylinders are plotted versus $\frac{R_t}{W}$. The maximum flux $\phi(r_o = R_e \, ; \, z_o = 0)$ is reached at about $\frac{R_t}{W} \approx 2$. Figure 6 shows the variation of the total number of neutrons per sec with $\frac{R_t}{W}$ that pass through the inner cylinder, the outer cylinder and through the end plates (top and bottom plates together). As would be expected from a linear device, the asymmetry between the inner and outer cylinders decreases when R_t is increased. But it becomes small only for very large R_t - values. For the standard case $\frac{R_t}{W} = 1.5$ the inner cylinder absorbs 22.6 %, the outer cylinder 68.6 % and the end plates together 8.8 % of the total neutron emission. For the asymptotic case $\frac{R_t}{W} \to \infty$ the corresponding values are about 44 %, 44 % and 12 %.

The factor η versus $\frac{R_t}{W}$ is shown in Fig.7. It does not depend sensitively on the torus radius R_t. The reduction of the mean wall loading to 57 % in the standard case is thus mainly due to the z_o-dependence of the flux, i.e. due to the half-width of about 2 b. The minimum of η is found at $\frac{R_t}{W} \approx 2$. According to Eq.(13) this is in agreement with the maximum of the flux $\phi(R_e \, ; \, 0)$ at $\frac{R_t}{W} \approx 2$ in Fig. 5, since ϕ_{av} does not depend on $\frac{R_t}{W}$.

It should be noted that the asymptotic results ($\frac{R_t}{W} \to \infty$) agree well with results from an analytic calculation and numerical evaluation for a straight device given in Appendix A.

4. SUMMARY AND CONCLUSIONS

The neutron flux distribution on the wall of a toroidal thermonuclear reactor with strongly elongated cross section has been calculated. A homogeneous intensity of the neutron source and a rectangular plasma cross section have been assumed. It is found that the flux is distributed in a very similar manner on the inner and on the outer cylinder, except, that the flux on the outer cylinder exceeds the corresponding values on the inner cylinder for all z_o. Both distributions have a plateau region that is symmetric to the $z_o = 0$ plane with a half-width of about the height of the plasma (2 b). As would be expected from geometrical arguments, the flux on the end plates is relatively small. The maximum flux is found on the outer cylinder and in the symmetry plane ($r_o = R_e$; $z_o = 0$).

The distribution of the asymmetry of flux has been computed for standard parameters ($\frac{R_i}{W} = 1$, $\frac{R_e}{W} = 2$, $\frac{H}{W} = 6$, $\frac{a}{W} = 0.2$, $\frac{b}{W} = 2.0$ and $\frac{R_t}{W} = 1.5$). A neutron flux clearly above the average value is found in the plateau region on the outer cylinder. The reduction factor η of the mean wall loading due to flux asymmetry is 57 % for standard parameters.

A variation of the torus radius with a fixed coil and plasma cross section has shown that η does not depend sensitively on toroidal curvature. Therefore, the reduction of the mean wall loading is mainly due to the decay of the flux along z_o with a half-width of about 2 b. The minimum of η at $\frac{R_t}{W} \approx 2$ is consistent with the maximum of ϕ ($r_o = R_e$; $z_o = 0$) for the same torus radius. It is found for the standard case with $\frac{R_t}{W} = 1.5$ that the inner cylinder absorbs 22.6 %, the outer cylinder 68.6 % and the end plates together 8.8 % of the total neutron emission. For the asymptotic case $\frac{R_t}{W} \to \infty$ the corresponding values are about 44 %, 44 % and 12 % in agreement with an analytic computation for a straight device. As would be expected, the asymmetry between the inner and outer cylinders decreases when R_t is increased. It is a

favourable feature of devices with strongly elongated cross sections that their flux asymmetry does not depend sensitively on the toroidal equilibrium position of the plasma.

References:

/1/ Daenner, W., Symp. on Reactor Technology, Grenoble (1972), 107

Appendix A

Neutron flux distribution on the wall of a straight device with elongated cross section

1) Method of calculation

It is assumed again that the intensity ε of the neutron source is homogeneous, and that the plasma has a rectangular cross section (see Fig. A 1). The linear device is assumed infinite and homogeneous in the y-direction, i.e. it is sufficient to calculate the flux distribution in a plane $y_o = 0$. (P_o (x_o, y_o, z_o) on the wall, $P(x, y, z)$ in the plasma). The centre of the plasma is assumed at $x = \frac{W}{2}$ and $z = 0$, and, therefore, the flux is distributed symmetrically to $x = \frac{W}{2}$ and $z = 0$. The calculation is only done with $x_o = 0$; $y_o = 0$ and $0 \leq z_o \leq \frac{H}{2}$ because we are mainly interested in the flux distribution on the vertical walls. This yields for the distance ℓ between P_o and P according to Eq. (2)

$$\ell^2 = x^2 + y^2 + (z - z_o)^2 \tag{A 1}$$

Now the appropriate coordinates are Cartesian coordinates x, y, z.

The angle α between the normal vector of a surface element df_o on the wall and the vector $\vec{\ell}$ is given by

$$\cos \alpha = \frac{x}{\ell} \tag{A 2}$$

This yields for the projection of df_o onto a plane perpendicular to $\vec{\ell}$

$$df = df_o \frac{x}{\ell} \tag{A 3}$$

The element $d\Omega$ of solid angle in which df_o appears as seen from a point P in the plasma is

$$d\Omega = \frac{df}{\ell^2} = df_o \frac{x}{\ell^3} \tag{A 4}$$

For the number of neutrons per sec that pass through df_o and that are emitted by a volume element $dV = dx\, dy\, dz$ of the source one obtains

$$d\phi(z_o)\, df_o = \frac{d\Omega}{4\pi}\, dV \cdot \varepsilon$$

and

$$d\phi(z_o)\, df_o = \frac{\varepsilon}{4\pi}\, df_o \frac{x\, dx\, dy\, dz}{[x^2 + y^2 + (z - z_o)^2]^{3/2}} \tag{A 5}$$

The neutron flux at $x_o = 0$, $y_o = 0$ and $z_o = z_o$ reads

$$\phi(z_o) = \frac{\varepsilon}{4\pi} \int\limits_{x=\frac{W}{2}-a}^{\frac{W}{2}+a} \int\limits_{y=-\infty}^{\infty} \int\limits_{z=-b}^{b} \frac{x \, dx \, dy \, dz}{\left[x^2 + y^2 + (z-z_o)^2\right]^{3/2}} \qquad (A\,6)$$

The y and z-integration can be done analytically:

$$\frac{2\pi}{\varepsilon}\phi(z_o) = \int\limits_{x=\frac{W}{2}-a}^{\frac{W}{2}+a} dx \, x \int\limits_{z=-b}^{b} dz \int\limits_{y=0}^{\infty} \frac{dy}{(y^2+k^2)^{3/2}}$$

with $k^2 = x^2 + (z-z_o)^2$.

$$\int\limits_{y=0}^{\infty} \frac{dy}{(y^2+k^2)^{3/2}} = \frac{y}{k^2\sqrt{y^2+k^2}} \Bigg|_o^\infty = \frac{1}{k^2}\lim_{y\to\infty}\frac{y}{\sqrt{y^2+k^2}} = \frac{1}{k^2}$$

This yields

$$\frac{2\pi}{\varepsilon}\phi(z_o) = \int\limits_{x=\frac{W}{2}-a}^{\frac{W}{2}+a} dx \, x \int\limits_{z=-b}^{b} \frac{dz}{x^2+(z-z_o)^2}$$

$$\int\limits_{z=-b}^{b} \frac{dz}{(z-z_o)^2+x^2} = \int\limits_{\varsigma=-b-z_o}^{b-z_o} \frac{d\varsigma}{\varsigma^2+x^2} = \frac{1}{x}\tan^{-1}\left(\frac{\varsigma}{x}\right)\Bigg|_{-b-z_o}^{b-z_o}$$

$$= \frac{1}{x}\left[\tan^{-1}\left(\frac{b-z_o}{x}\right) + \tan^{-1}\left(\frac{b+z_o}{x}\right)\right]$$

with $\varsigma = z - z_o$

$$\phi(z_o) = \frac{\epsilon}{2\pi} \left[\int\limits_{x=\frac{W}{2}-a}^{\frac{W}{2}+a} \tan^{-1}\left(\frac{b-z_o}{x}\right) dx + \int\limits_{x=\frac{W}{2}-a}^{\frac{W}{2}+a} \tan^{-1}\left(\frac{b+z_o}{x}\right) dx \right] \qquad (A\ 7)$$

The x-integrals are evaluated numerically for $\epsilon = 1$ and the standard parameters:

$$\frac{H}{W} = 6, \quad \frac{a}{W} = 0.2 \text{ and } \quad \frac{b}{W} = 2.0$$

The results are given in Fig. A 2.

Figure Captions

Fig. 1   Coil and plasma geometry.

Fig. 2   Geometrical quantities used in the calculation of the neutron flux distribution.

Fig. 3   Neutron flux distributions on a) inner wall (ϕ_i); b) external wall (ϕ_e) and
c) top or bottom plate (ϕ_p) for standard parameters.

Fig. 4   Asymmetry factors   for the standard case on
a) inner wall (Δ_i); b) outer wall (Δ_e); c) top or bottom plate (Δ_p) .

Fig. 5   Neutron fluxes ϕ in the $z_o = 0$ plane on the inner cylinder (dashed curve) and on
the outer cylinder versus $\frac{R_t}{W}$.

Fig. 6   Total current of neutrons $\frac{\psi}{\psi_{tot}}$ through the inner cylinder (dashed curve), the
outer cylinder (solid curve) and the top and bottom plates together (dotted
curve) versus $\frac{R_t}{W}$.

Fig. 7   Reduction factor η versus $\frac{R_t}{W}$.

Fig. A 1 Coil and plasma geometry for a straight device.

Fig. A 2 Neutron flux distribution on a vertical wall of a straight device.
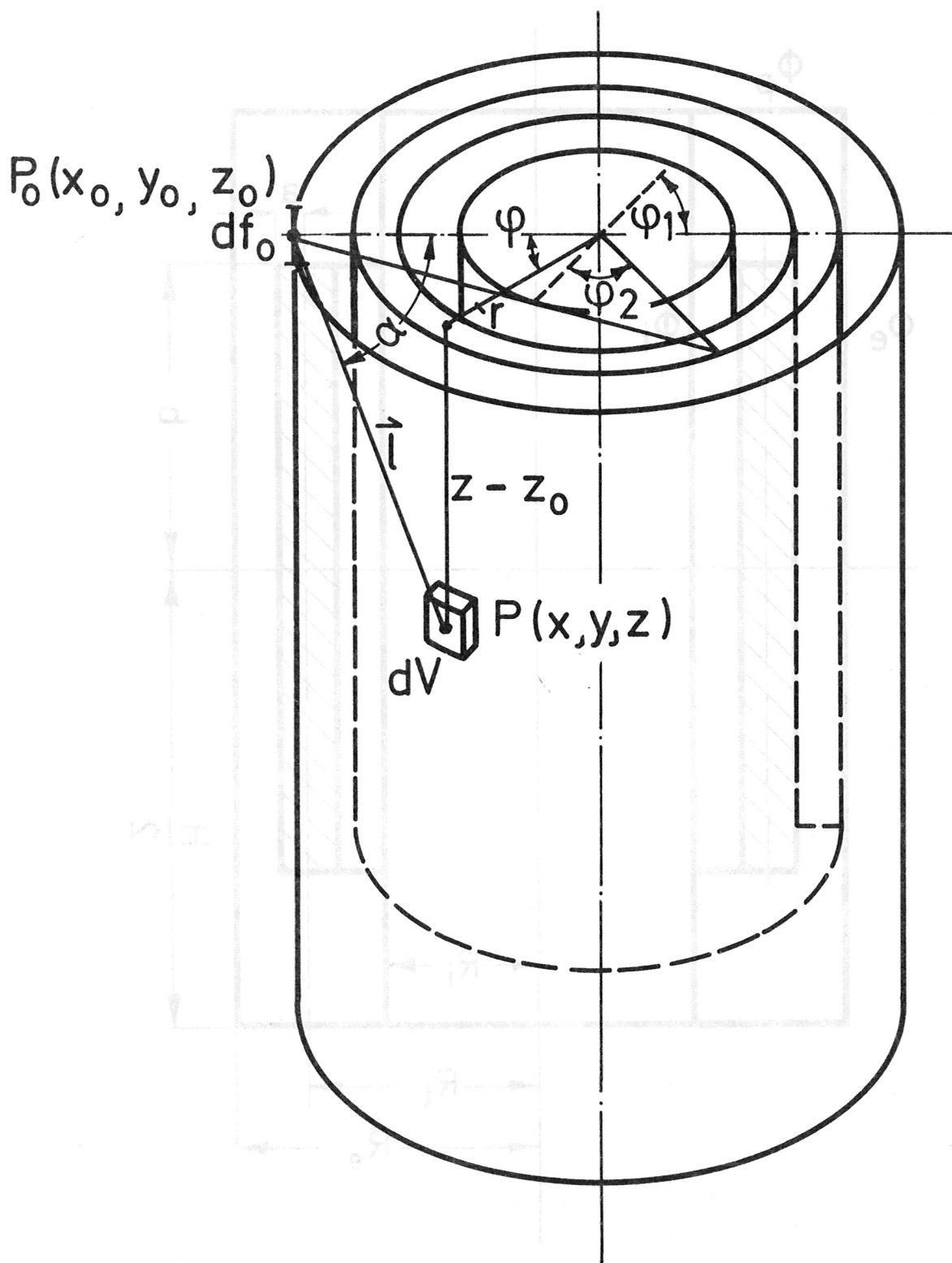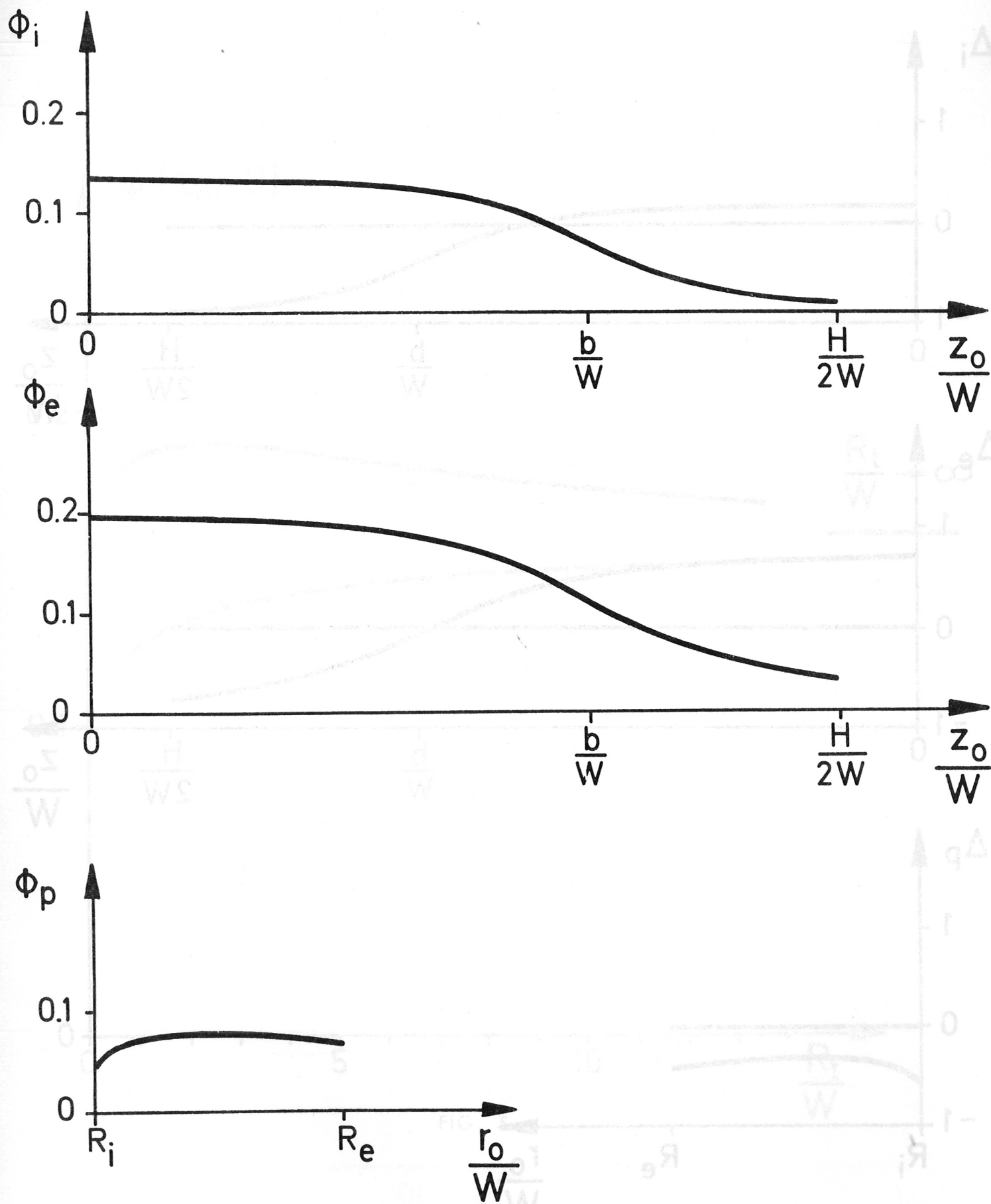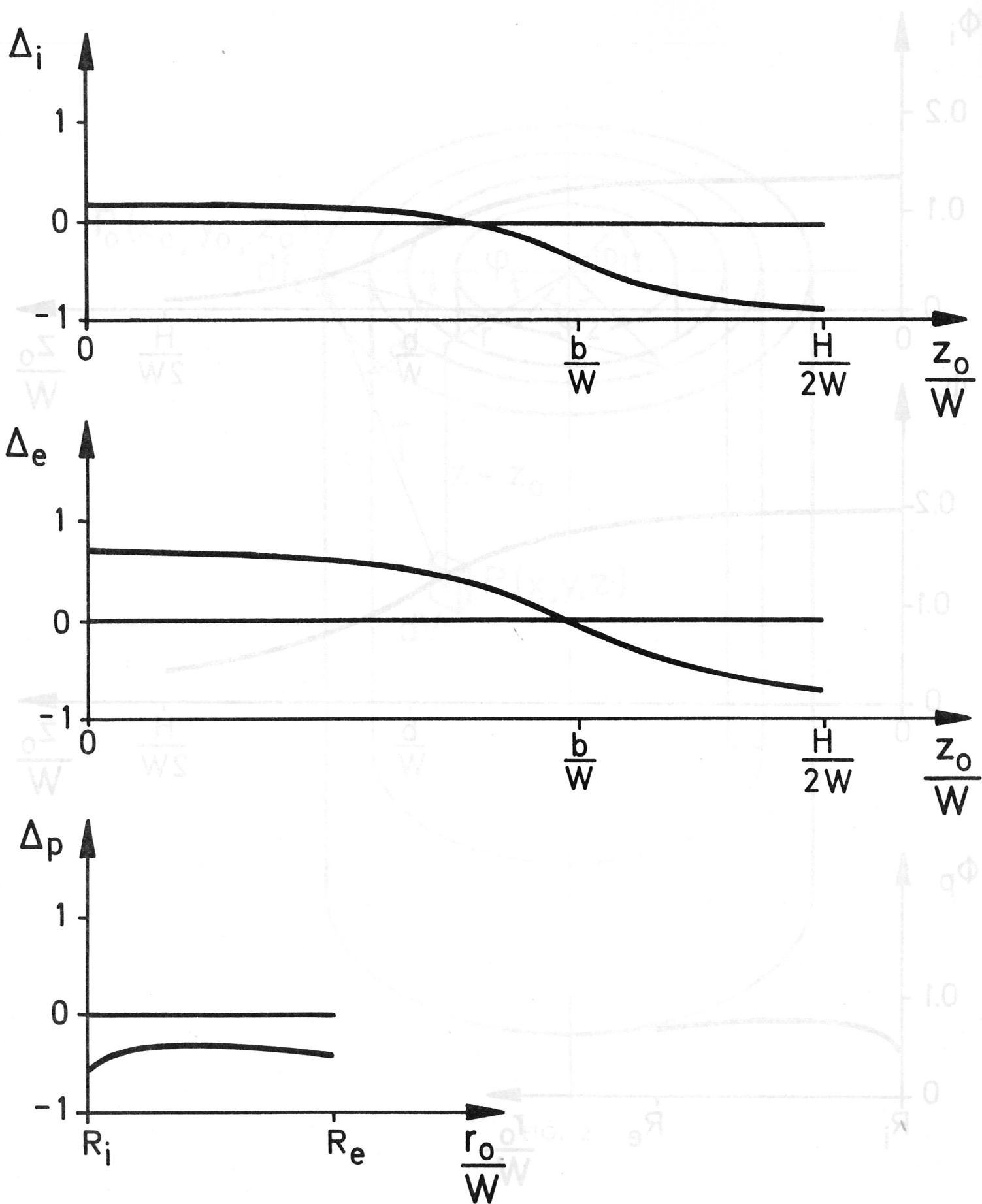
Φ_p

Φ_e

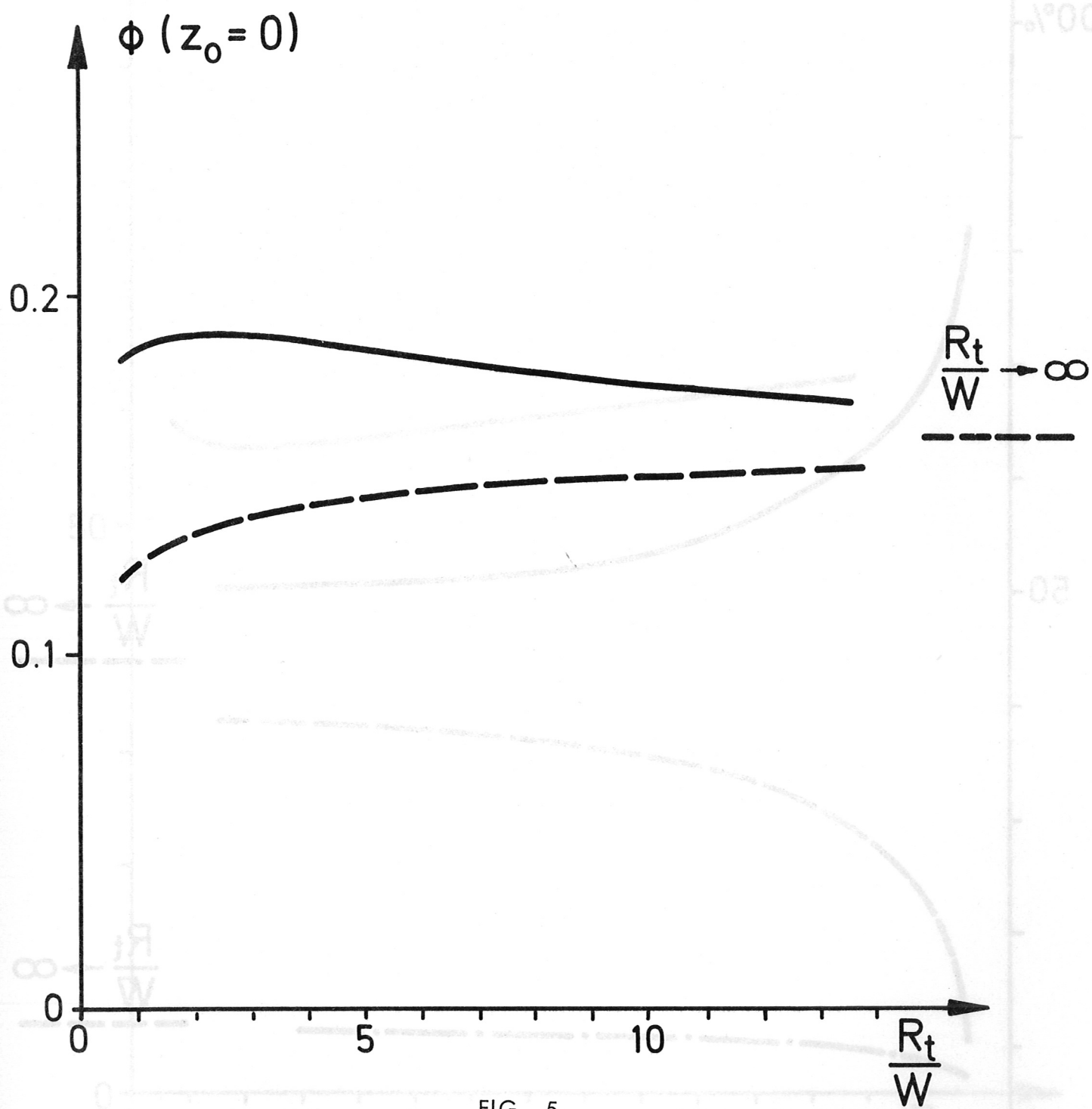Φ_i

a

b

$\frac{H}{2}$

R_i

R_t

R_e

FIG. 1

FIG. 2

FIG. 3

FIG. 4

FIG. 5

FIG. 6

FIG. 7

FIG. A 1

FIG. A 2